Supporting Information

Interfacially coupled thin sheet-like NiO/$NiMoO_4$ nanocomposites synthesized by simple reflux method for excellent electrochemical performance

Achal Singh Keshari and Prashant Dubey*

Centre of Material Sciences, Institute of Interdisciplinary Studies, University of Allahabad, Prayagraj-211002 (U.P.), INDIA

Email: pdubey@allduniv.ac.in, pdubey.au@gmail.com

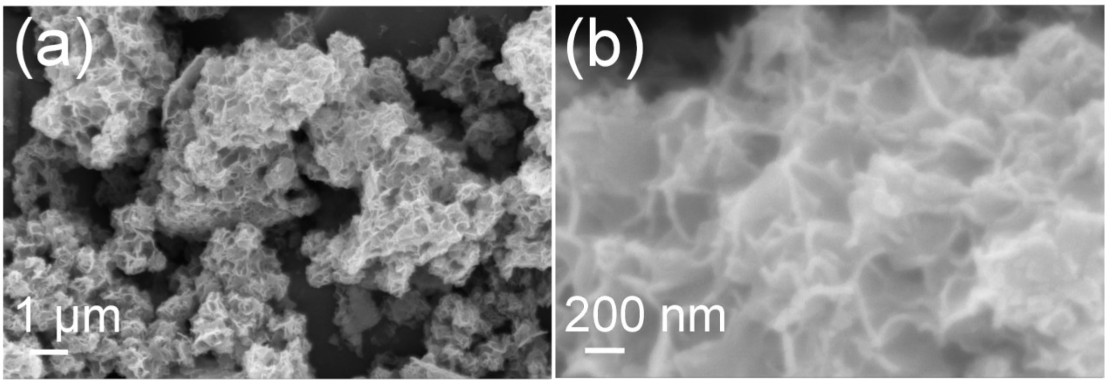

Fig. S1 FESEM micrographs of Ni-Mo hydroxide precursor synthesized during 10 h reflux time. Low-magnification **(a)** and corresponding high-magnification **(b)**.

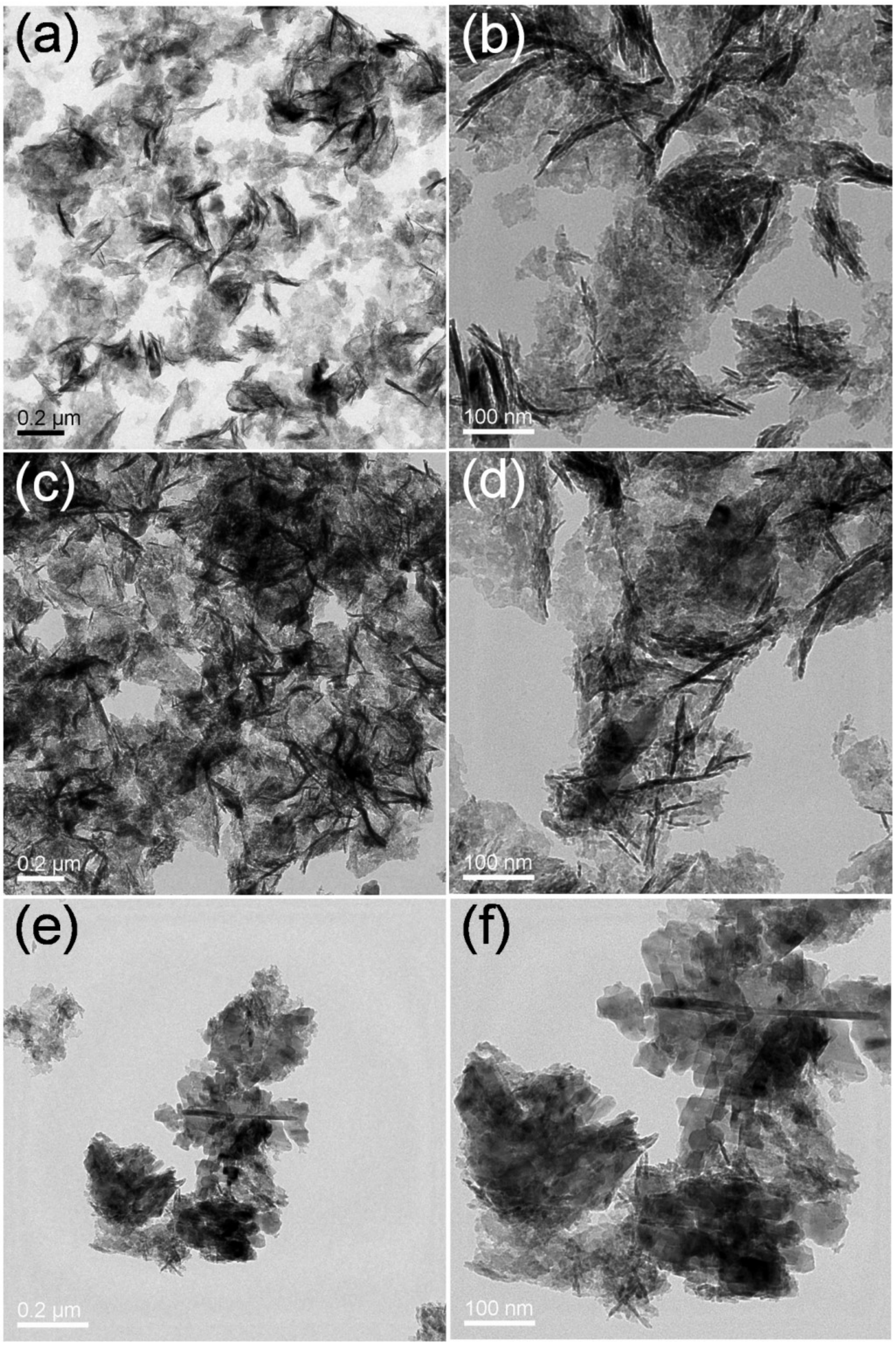

Fig. S2 Different magnification TEM images of NNMO-1 **(a, b)**, NNMO-2 **(c, d)**, and NNMO-4 **(e, f)** nanocomposites.

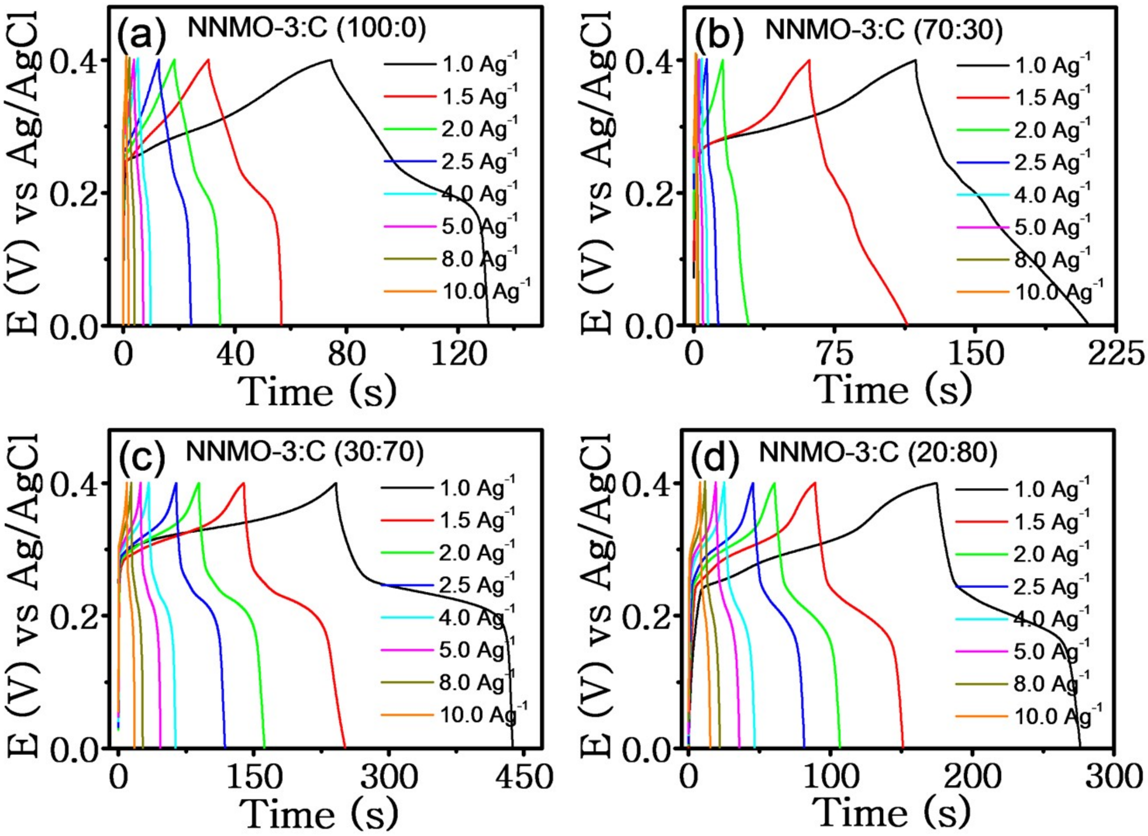

Fig. S3 GCD curves according to different specific currents of 1.0 to 10.0 Ag^{-1} for different combinations of NNMO-3: C as 100: 0 **(a)**, 70: 30 **(b)**, 30: 70 **(c)**, and 20: 80 **(d)**. **(Color)**

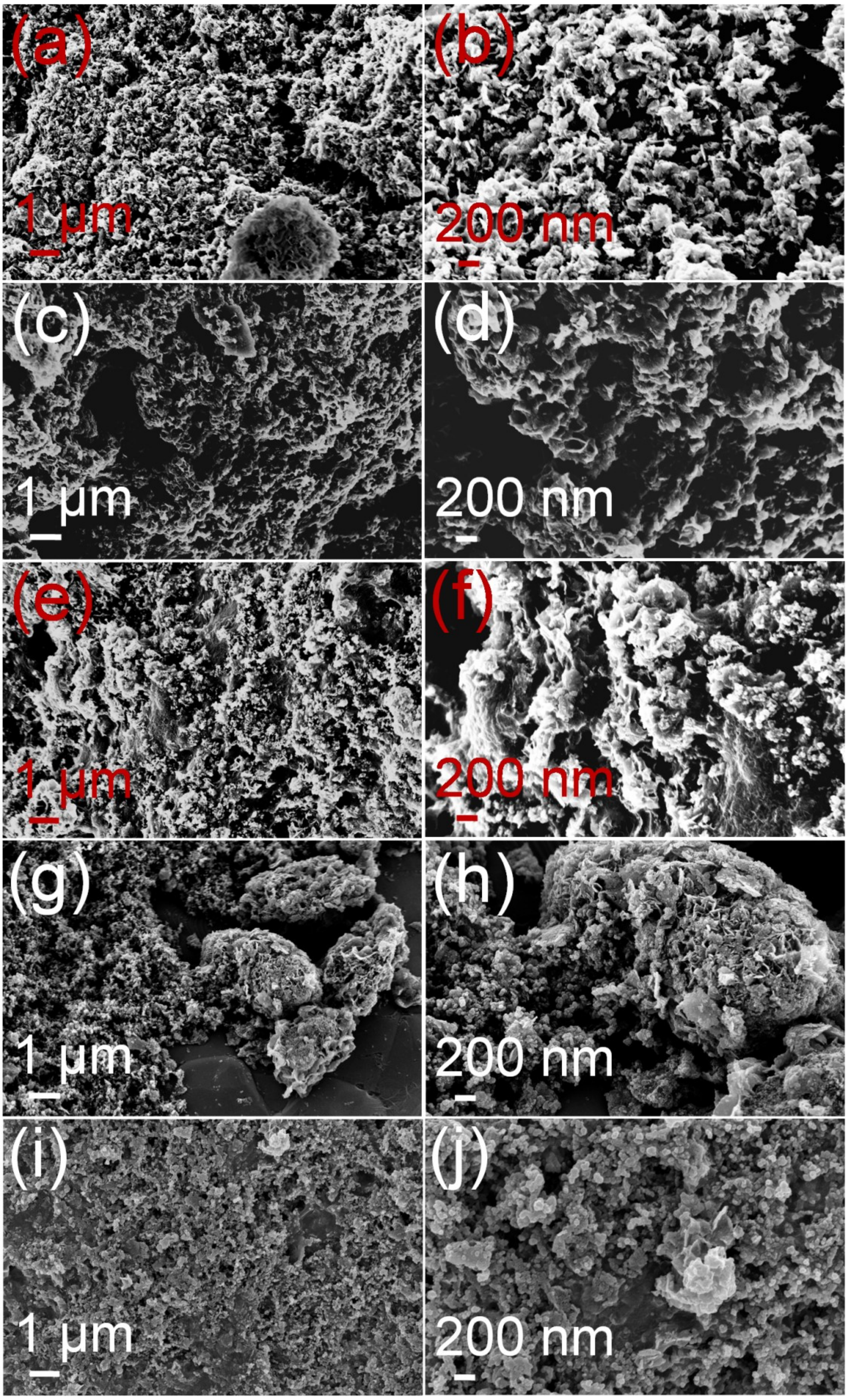

Fig. S4 Low- and corresponding high-magnification SEM micrographs of fabricated working electrodes according to different combinations of NNMO-3: C as 100: 0 **(a, b)**, 70: 30 **(c, d)**, 50: 50 **(e, f)**, 30: 70 **(g, h)**, and 20: 80 **(i, j)**.

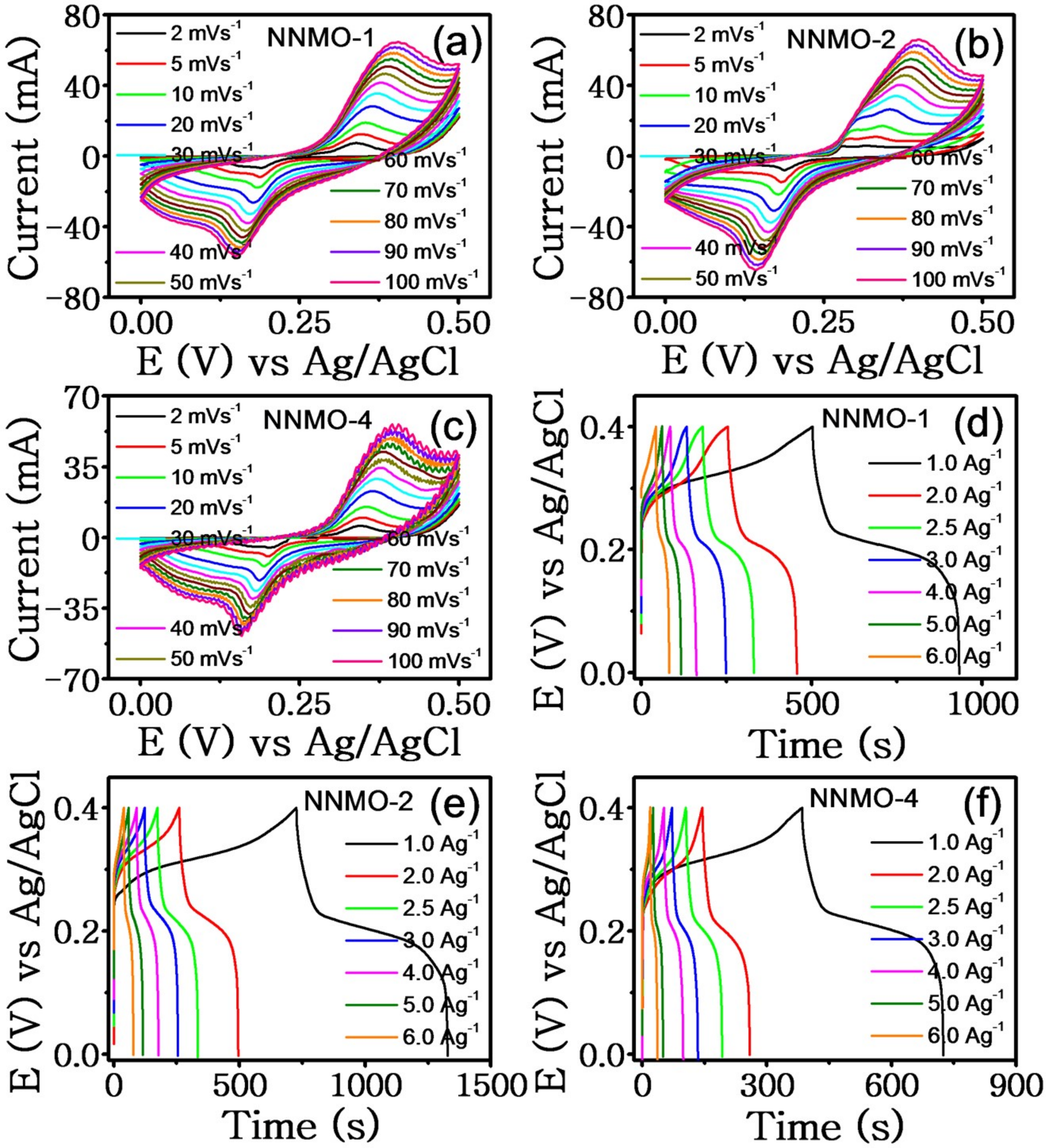

Fig. S5 CV curves at different scan rates (2 to 100 mVs^{-1}) **(a, b, c)** and GCD curves at various specific currents (1.0 to 6.0 Ag^{-1}) **(d, e, f)** of NNMO-1, NNMO-2, and NNMO-4 electrodes, respectively. **(Color)**

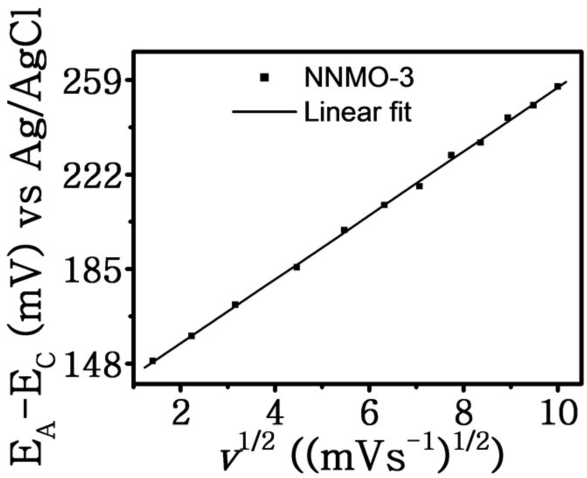

Fig. S6 Linear fitted plot of peak potential difference (anodic and cathodic) as a function of square root of scan rates for NNMO-3 electrode.

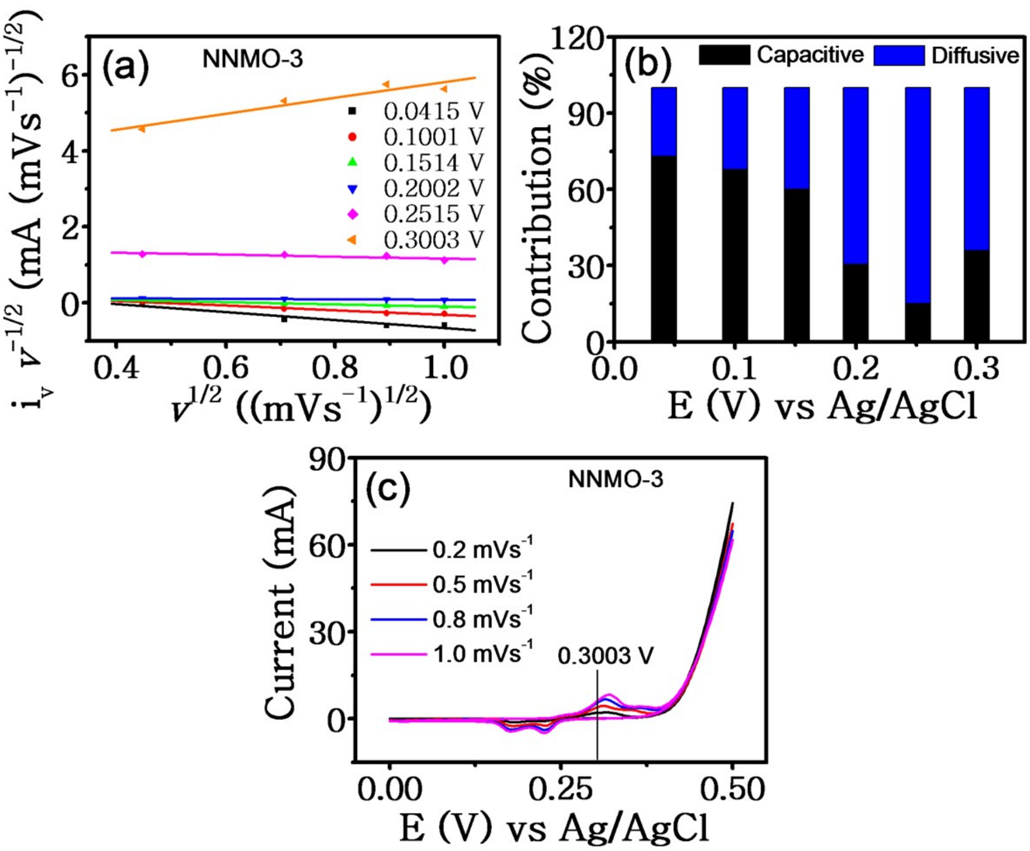

Fig. S7 Linear fitted plots of scan rate $(\upsilon)^{1/2}$ as a function of $i_v\ \upsilon^{-1/2}$ for NNMO-3 electrode at different fixed potentials obtained from slow scan rate CV curves (0.2 to 1 mVs^{-1}) **(a, c)** and corresponding bar diagram of capacitive/ diffusive contributions **(b)**. **(Color)**

Estimation of electrochemical active surface area (ECASA):

The ECASA of the fabricated nanocomposite electrodes (NNMO-1, NNMO-2, NNMO-3, and NNMO-4) is estimated from CV measurements within a potential window of 0 to 0.5 V (vs Ag/AgCl) at different scan rates (2, 5, 10, 20, 30, 40, 50, 60, 70, 80, 90, and 100 mVs^{-1}). Plots of current response (mA) with respect to scan rate of all the tested electrodes for a particular potential of 0.0415 V (vs Ag/AgCl) are shown in Fig. S8, which follow linear relationships. The double-layer capacitance (C_{dl}) at non-Faradic region by adsorption of electrolytic ions is calculated from the slope of current response as a function of scan rate at a particular potential according to the following relationship [1, 2]:

$$i = C_{dl}\frac{dV}{dt}$$

Where i (A) is the response current at a fixed potential, $\frac{dV}{dt}$ (mVs^{-1}) is the scan rate, and C_{dl} (F) is the double-layer capacitance.

Furthermore, C_{dl} can be correlated to ECASA as follows [1, 2].

$$ECASA = \frac{C_{dl}}{C_s}$$

where C_s is the generalized capacitance in KOH aqueous medium (20 μFcm^{-2}).

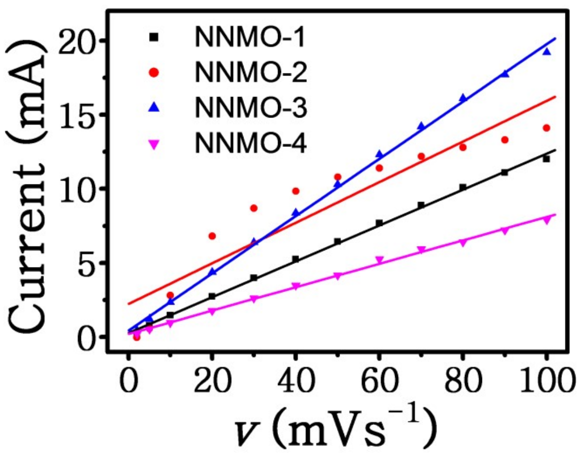

Fig. S8 Linear fitted plots of response currents as a function of scan rates for all the tested nanocomposite electrodes. **(Color)**

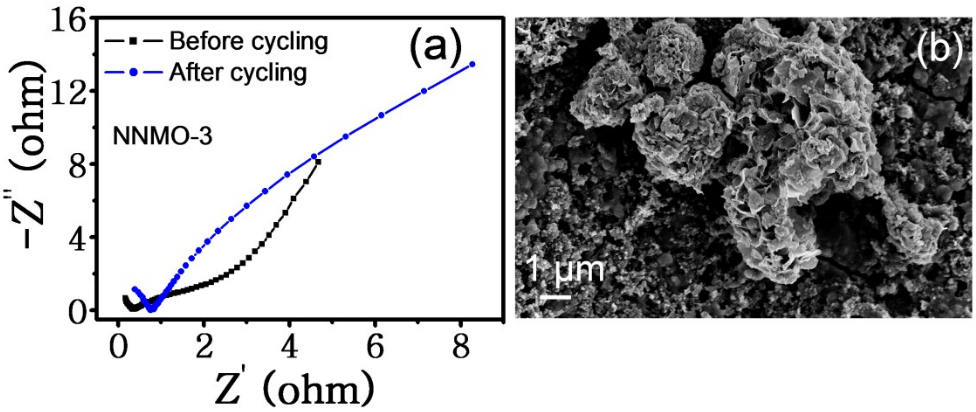

Fig. S9 Nyquist plots of NNMO-3 electrode before and after cycling experiment **(a)** and corresponding FESEM micrograph after 2200 cycling test **(b)**. **(Color)**

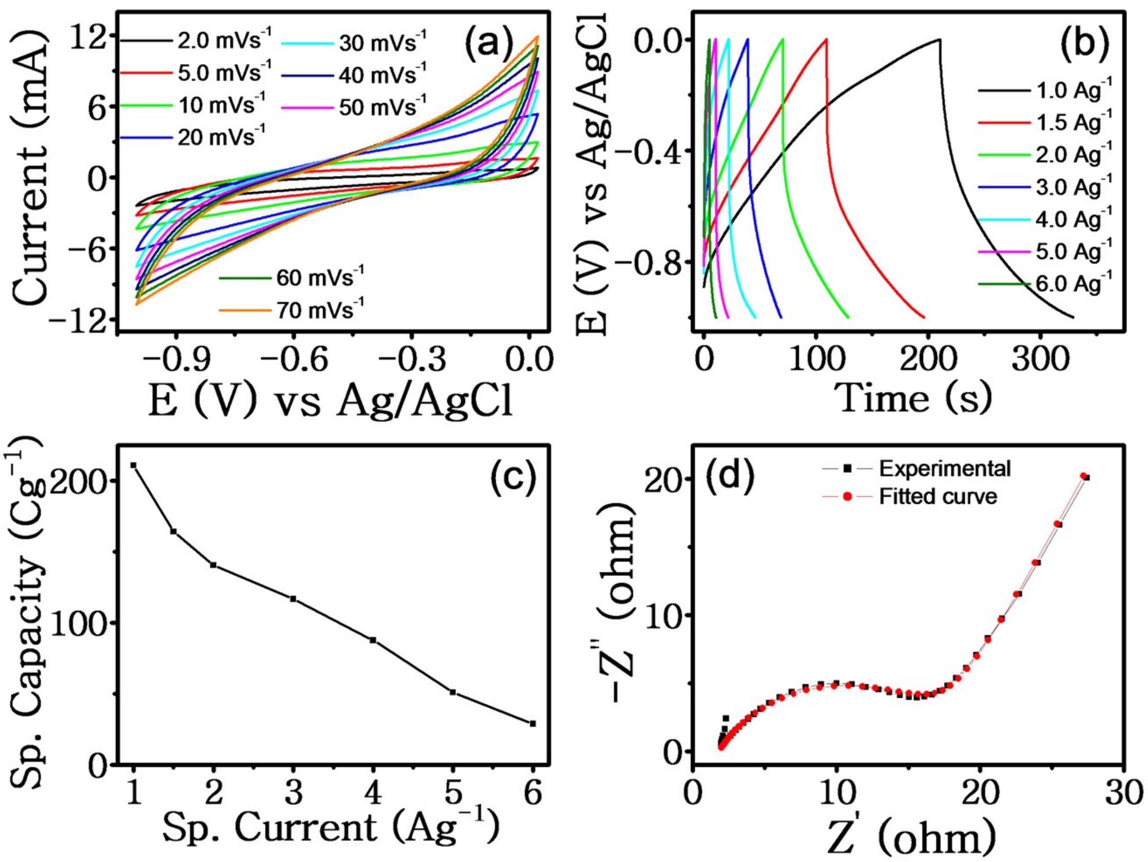

Fig. S10 CV curves at various scan rates of 2 to 70 mVs^{-1} **(a)**, GCD plots according to varying specific currents **(b)**, specific capacity as a function of specific current **(c)**, and Nyquist plot **(d)** of AC electrode material. **(Color)**

Table S1. Structural parameters of NNMO nanocomposites calculated from XRD profiles.

Materials	Phase content (%) corresponding to (220) plane			d spacing (nm) corresponding to (220) plane			Crystallite size, D_p (nm) corresponding to (220) plane		
	α-NMO	β-NMO	NiO	α-NMO	β-NMO	NiO	α-NMO	β-NMO	NiO
NNMO-1	40.6	18.2	41.2	0.310	0.334	0.15	21.3	25.4	6.6
NNMO-2	27.6	19.6	52.8				17.9	16.9	6.7
NNMO-3	23.7	18.7	57.6				22.6	20.7	7.7
NNMO-4	18.0	12.1	69.9				17.9	15.3	8.3

Table S2. Planes corresponding to different rings in the SAED pattern.

Rings	1/2r, (1/nm)	1/r	r (nm)/ d spacing	d (Å)	(hkl)	Phase
1	3.26	1.63	0.613497	6.134969	(110)	α-NMO
2	5.221	2.6105	0.383068	3.830684	(02-1)	β-NMO
3	6.456	3.228	0.309789	3.097893	(220)	α-NMO
4	8.194	4.097	0.244081	2.44081	(111)	NiO
5	9.574	4.787	0.208899	2.088991	(200)	NiO
6	12.434	6.217	0.160849	1.608493	(024)	α-NMO
7	13.558	6.779	0.147514	1.475144	(220)	NiO
8	16.607	8.3035	0.120431	1.204311	(222)	NiO
9	19.215	9.6075	0.104085	1.040853	(400)	NiO
10	21.39	10.695	0.093502	0.935016	(420)	NiO
11	23.49	11.745	0.085143	0.851426	(1022)	β-NMO

Table S3. The calculated value of specific capacities from CV and GCD curves for different combinations of NNMO-3: C electrodes.

Electrode materials	Sp. capacity, Q_1 (Cg^{-1}) at 2.0 mVs^{-1}	Sp. capacity, Q_1 (Cg^{-1}) at 30.0 mVs^{-1}	Sp. capacity, Q_2 (Cg^{-1}) at 1.0 Ag^{-1}	Sp. capacity, Q_2 (Cg^{-1}) at 10.0 Ag^{-1}	Capacitive retention (%)
NNMO-3:C (100:0)	121.2	138.0	56.2	8.0	14.2
NNMO-3:C (70:30)	230.8	76.1	92.4	6.0	6.5
NNMO-3:C (50:50)	877.7	432.1	649.8	276.0	42.5
NNMO-3:C (30:70)	182.1	111.6	195.9	84.0	42.9
NNMO-3:C (20:80)	83.9	73.9	101.1	71.0	70.2

Table S4. The calculated value of specific capacities from CV and GCD curves for different NNMO nanocomposite electrodes.

Electrode materials	Sp. capacity, Q_1 (Cg^{-1}) at 2.0 mVs^{-1}	Sp. capacity, Q_1 (Cg^{-1}) at 30.0 mVs^{-1}	Sp. capacity, Q_2 (Cg^{-1}) at 1.0 Ag^{-1}
NNMO-1	548.6	270.1	430.1
NNMO-2	813.3	261.7	601.1
NNMO-3	877.7	432.1	649.8
NNMO-4	401.5	208.8	340.2

Table S5. The capacitive and diffusive contributions of NNMO-3 electrode from slow scan rate CV curves (0.2 to 1.0 mVs^{-1}) at various fixed potentials.

Potential (V) vs Ag/AgCl	NNMO-3	
	Slope, k1 (%)	Intercept, k2 (%)
0.0415	-1.060 (72.9)	0.395 (27.1)
0.1001	-0.603 (67.7)	0.288 (32.3)
0.1514	-0.308 (60.1)	0.205 (39.9)
0.2002	-0.063 (30.4)	0.144 (69.6)
0.2515	-0.248 (14.9)	1.413 (85.1)
0.3003	2.081 (35.8)	3.726 (64.2)

Table S6. Comparison of electrochemical performance (in the three-electrode system) of the NNMO-3 electrode with reported NMO based binder-free nanocomposite/ hybrid electrode materials.

Electrode materials	Synthetic method	Specific surface area (m^2g^{-1})	Sp. capacitance (Fg^{-1}) @ Sp. current (Ag^{-1})	Capacitive retention (%) @ Number of cycles (Sp. current/ Ag^{-1})	Ref.
$Co_3O_4/NiMoO_4$ core/shell nanowire arrays@NF	H, C	—	1230.0 @ 1.9	77.0 @ 3000 (9.6)	[3]
3D $Co_3O_4/NiMoO_4$ nanocomposites@NF	H, C	—	2041.0 @ 0.5	72.0 @ 3000 (0.5)	[4]
$CoMoO_4/NiMoO_4{\cdot}xH_2O$ core-shell heterostructure@CF	H, C	100.8	1582.0 @ 1.0	97.1 @ 3000 (1.0)	[5]
$Ni_{0.75}Co_{0.25}MoO_4$ porous nanosheets@CC	H, C	—	1321.1 @ 1.0	97.2 @ 3000 (5.0)	[6]
$NiMoO_4$/Ni-Co-S core-shell nanorods@NF	H, C	—	1892.0 @ 5.0*	91.7 @ 6000 (20.0*)	[7]
$NiMoO_4/NiWO_4$ honeycomb@NF	H, C	—	1290.0 @ 2.0	93.1 @ 3000 (6.0)	[8]
$NiO/NiCo_2O_4$ core-shell nanosheet arrays@NF	H, C	—	1623.6 @ 2.0	90.0 @ 10,000 (10.0)	[9]
$NiCo_2S_4/NiMoO_4$ core-shell nanosheet arrays@NF	H	—	1487.6 @ 1.0	89.7 @ 8000 (5.0)	[10]
$MgCo_2O_4/NiMoO_4$ urchin-like core-shell nanomaterial@NF	H, C	—	1775.0 @ 1.0	74.7 @ 5000 (5.0)	[11]

$MnCo_2O_4/NiMoO_4$ core-shell nanowire array@NF	H, C	119.2	1244.0 @ 1.0	81.0 @ 2500 (5.0)	[12]
$NiCo_2O_4$@$NiMoO_4$/PANI holothurian@CC	H, C, P	—	1322.2 @ 0.6	92.36 @ 5000 (0.6)	[13]
$NiCo_2O_4$@$NiMoO_4$ nanowires/nanosheets array@CC	H, C	272.3	1576.0 @ 1.0	89.8 @ 5000 (3.3)	[14]
$CuCo_2O_4/NiMoO_4$ nanoarchitecture@NF	H, C	—	2215.0 @ 1.0	98.3 @ 8000 (5.0)	[15]
$NiCo_2O_4/NiMoO_4$ nanostructure@NF	H, C	—	1371.4 @ 1.0	100 @ 10,000 (8.0)	[16]
NiCoMn–O@$NiMoO_4$@C nanosheet arrays@CC	H, C	—	2189.5 @ 0.25	81.6 @ 1500 (6.0)	[17]
$ZnCo_2O_4$@$NiMoO_4$ core-shell nanowire/nanosheets nanoarrays@NF	H, C	—	1912.0 @ 1.0	—	[18]
$NiMoO_4/NiSe_2/MoSe_2$ nanowire@GCE	H, C, Se	55.6	955.0 @ 1.0	86.1 @ 5000 (10.0)	[19]
NNMO-3 sheet-like nanocomposite	Reflux, C	113.0	1624.5 @ 1.0	73.5 @ 2200 (1.0)	This work

NF: Ni foam; CF: Carbon fabric; CC: Carbon cloth, GCE: Glassy carbon electrode; H: Hydrothermal; C: Calcination/ Annealing; P: Polymerization; Se: Selenylation; *: $mAcm^{-2}$.

Table S7. The calculated values of C_{dl} and ECASA for different nanocomposite electrodes.

Electrode material	Double-layer capacitance, C_{dl} (mF)	ECASA (cm^2)
NNMO-1	120.6	6031.3
NNMO-2	137.3	6863.2
NNMO-3	193.0	9650.1
NNMO-4	79.0	3949.0

Table S8. Various fitting parameters and values obtained from EIS measurements of all the tested nanocomposite electrodes.

Electrode materials	R_s (Ω)	R_{ct} (Ω)	CPE in low frequency region		Impedance (Ω)	- Phase angle (intercept of –Z″ axis at 0.1 Hz)
			Y_0 (Ω^{-1})	n		
NNMO-1	1.15	15.21	0.07	0.56	32.35	30.2
NNMO-2	0.34	8.53	0.08	0.74	23.21	48.6
NNMO-3	0.32	3.07	0.19	0.88	9.36	60.1
NNMO-4	1.06	24.0	0.08	0.37	36.67	15.9
NNMO-3 (after cycling)	0.76	7.61	0.14	0.73		

Table S9. The calculated values of specific capacity, specific energy and specific power of NNMO-3//AC ASC device.

ASC device	Sp. capacity, Q_1 (Cg^{-1}) at 2.0 mVs^{-1}	Sp. capacity, Q_2 (Cg^{-1}) at 1.0 Ag^{-1}	Sp. capacity, Q_2 (Cg^{-1}) at 5.0 Ag^{-1}	Capacitive retention (%) from 1.0 to 5.0 Ag^{-1}	Sp. energy, *E* ($Whkg^{-1}$)	Sp. power, *P* (Wkg^{-1})
NNMO-3// AC	222.9	216.2	126.5	58.5	45.0 @ 1.0 Ag^{-1} 26.4 @ 5.0 Ag^{-1}	750.0 @ 1.0 Ag^{-1} 3750.0 @ 5.0 Ag^{-1}

Table S10. Fitting parameters like R_s, R_{ct}, n of the NNMO-3//AC ASC device obtained from Nyquist plots before and after cycling test.

Parameters→	**R_s (Ω)**	**R_{ct} (Ω)**	**n**
Before cycling	1.15	15.21	0.64
After cycling	8.75	19.68	0.50

References

1. C. C. L. McCrory, S. Jung, I. M. Ferrer, S. M. Chatman, J. C. Peters and T. F. Jaramillo, Benchmarking hydrogen evolving reaction and oxygen evolving reaction electrocatalysts for solar water splitting devices, *J. Am. Chem. Soc.*, 2015, **137**, 4347−4357.
2. G. P. Sharma, P. K. Gupta, S. K. Sharma, R. G. S Pala and S. Sivakumar, Chalcogenide dopant-induced lattice expansion in cobalt vanadium oxide nanosheets for enhanced supercapacitor performance, *ACS Appl. Energy Mater.*, 2021, **4**, 4758−4771.
3. D. Cai, D. Wang, B. Liu, L. Wang, Y. Liu, H. Li, Y. Wang, Q. Li and T. Wang, Three dimensional Co_3O_4@$NiMoO_4$ core/shell nanowire arrays on Ni foam for electrochemical energy storage, *ACS Appl. Mater. Interfaces*, 2014, **6**, 5050−5055.
4. X. J. Ma, L. B. Kong, W. B. Zhang, M. C. Liu, Y. C. Luo and L. Kang, Design and synthesis of 3D Co_3O_4@$MMoO_4$ (M=Ni, Co) nanocomposites as high-performance supercapacitor electrodes, *Electrochim. Acta*, 2014, **130**, 660−669.
5. J. Wang, L. Zhang, X. Liu, X. Zhang, Y. Tian, X. Liu, J. Zhao and Y. Li, Assembly of flexible $CoMoO_4$@$NiMoO_4\cdot xH_2O$ and Fe_2O_3 electrodes for solid-state asymmetric supercapacitors, *Scientific Reports*, 2017, **7**, 41088.
6. P. Sun, C. Wang, W. He, P. Hou and X. Xu, One-step synthesis of 3D network-like $Ni_xCo_{1-x}MoO_4$ porous nanosheets for high performance battery-type hybrid supercapacitors, *ACS Sustainable Chem. Eng.*, 2017, **5**, 10139−10147.
7. C. Chen, D. Yan, X. Luo, W. Gao, G. Huang, Z. Han, Y. Zeng and Z. Zhu, Construction of core-shell $NiMoO_4$@Ni-Co-S nanorods as advanced electrodes for high-performance asymmetric supercapacitors, *ACS Appl. Mater. Interfaces*, 2018, **10**, 4662−4671.
8. A. E. Reddy, T. Anitha, C. V. V. M. Gopi, S. S. Rao and H. J. Kim, $NiMoO_4$@$NiWO_4$ honeycombs as a high performance electrode material for supercapacitor applications, *Dalton Trans.*, 2018, **47**, 9057−9063.

9. D. Yao, Y. Ouyang, X. Jiao, H. Ye, W. Lei, X. Xia, L. Lu and Q. Hao, Hierarchical $NiO@NiCo_2O_4$ core−shell nanosheet arrays on Ni foam for high-performance electrochemical supercapacitors, *Ind. Eng. Chem. Res.*, 2018, **57**, 6246−6256.
10. S. Chen, Z. Zhang, W. Zeng, J. Chen and L. Deng, Construction of $NiCo_2S_4@NiMoO_4$ core-shell nanosheet arrays with superior electrochemical performance for asymmetric supercapacitors, *Chem. Electro. Chem.*, 2019, **6**, 590−597.
11. H. Gao, X. Wang, G. Wang, C. Hao, C. Huang and C. Jiang, Facile construction of a $MgCo_2O_4@NiMoO_4$/NF core–shell nanocomposite for high-performance asymmetric supercapacitors, *J. Mater. Chem. C*, 2019, **7**, 13267−13278.
12. J. A. A. Mehrez, K. A. Owusu, Q. Chen, L. Li, K. Hamwi, W. Luo and L. Mai, Hierarchical $MnCo_2O_4@NiMoO_4$ as free-standing core-shell nanowire arrays with synergistic effect for enhanced supercapacitor performance, *Inorg. Chem. Front.*, 2019, **6**, 857−865.
13. J. Shen, Q. Wang, K. Zhang, S. Wang, L. Li, S. Dong, S. Zhao, J. Chen, R. Sun, Y. Wang, Z. Jian and W. Zhang, Flexible carbon cloth based solid-state supercapacitor from hierarchical holothurian-morphological $NiCo_2O_4@NiMoO_4$/PANI, *Electrochim. Acta*, 2019, **320**, 134578.
14. H. Zhang, C. Lu, H. Hou, Y. Ma and S. Yuan, Tuning the electrochemical performance of $NiCo_2O_4@NiMoO_4$ core-shell heterostructure by controlling the thickness of the $NiMoO_4$ shell, *Chem. Eng. J.*, 2019, **370**, 400–408.
15. G. Li, B. Song, X. Cui, H. Ouyang, K. Wang, Y. Sun and Y. Wang, Multidimensional and binary micro $CuCo_2O_4$/nano $NiMoO_4$ for high-performance supercapacitors, *ACS Sustainable Chem. Eng.*, 2020, **8**, 1687−1694.
16. D. Cui, R. Zhao, J. Dai, J. Xiang and F. Wu, Hybrid $NiCo_2O_4@NiMoO_4$ structure for overall water splitting and excellent hybrid energy storage, *Dalton Trans.*, 2020, **49**, 9668−9679.
17. X. Tang, Y.H. Lui, B. Zhang and S. Hu, Venus flytrap-like hierarchical NiCoMn–$O@NiMoO_4@C$ nanosheet arrays as free-standing core-shell electrode material for hybrid supercapacitor with high electrochemical performance, *J. Power Sources*, 2020, **477**, 228977.
18. J. Wang, S. Wang, Y. Tian, X. Jin and J. Dong, 3D heterogeneous $ZnCo_2O_4@NiMoO_4$ nanoarrays grown on Ni foam as a binder-free electrode for high-performance energy storage, *J. Energy Storage*, 2020, **32**, 101899.

19. C. Wang, D. Wu, Y. Qin and Y. Kong, Nanowired $NiMoO_4/NiSe_2/MoSe_2$ prepared through in situ selenylation as a high performance supercapacitor electrode, *Chem. Commun.*, 2021, **57**, 4019−4022.